CrossMark

Unmanned aerial vehicle (UAV)-based monitoring of a landslide: Gallenzerkogel landslide (Ybbs-Lower Austria) case study

Remzi Eker · Abdurrahim Aydın · Johannes Hübl

Abstract In the present study, UAV-based monitoring of the Gallenzerkogel landslide (Ybbs, Lower Austria) was carried out by three flight missions. High-resolution digital elevation models (DEMs), orthophotos, and density point clouds were generated from UAV-based aerial photos via structure-from-motion (SfM). According to ground control points (GCPs), an average of 4 cm root mean square error (RMSE) was found for all models. In addition, light detection and ranging (LIDAR) data from 2009, representing the prefailure topography, was utilized as a digital terrain model (DTM) and digital surface model (DSM). First, the DEM of difference (DoD) between the first UAV flight data and the LIDAR-DTM was determined and according to the generated DoD deformation map, an elevation difference of between − 6.6 and 2 m was found. Over the landslide area, a total of 4380.1 m^3 of slope material had been eroded, while 297.4 m^3 of the material had accumulated within the most active part of the slope. In addition, 688.3 m^3 of the total eroded material had belonged to the road destroyed by the landslide. Because of the vegetation surrounding the landslide area, the Multiscale Model-to-Model Cloud Comparison (M3C2) algorithm was then applied to compare the first and second UAV flight data. After eliminating both the distance uncertainty values of higher than 15 cm and the nonsignificant changes, the M3C2 distance obtained was between − 2.5 and 2.5 m. Moreover, the high-resolution orthophoto generated by the third flight allowed visual monitoring of the ongoing control/stabilization work in the area.

Keywords Landslide monitoring · M3C2 · DoD · SfM · UAV

R. Eker (✉) · A. Aydın
Faculty of Forestry, Düzce University, Konuralp Campus,
81620 Düzce, Turkey
e-mail: remzieker@duzce.edu.tr

A. Aydın
e-mail: aaydin@duzce.edu.tr

J. Hübl
Institute of Mountain Risk Engineering, University of Natural
Resources and Life Sciences, Peter Jordan-Straße 82,
A-1190 Wien, Austria
e-mail: johannes.huebl@boku.ac.at

Introduction

The understanding of landslides and their mechanisms is crucial for the reduction of landslide hazards, for human safety and for protection of civil infrastructures because "…the reduction of landslide hazard not only depends on spatio-temporal information about frequency and distribution of landslides, and of their predisposing and triggering factors, but also on the quantification and understanding of landslide kinematics and the underlying mechanical processes" (Stumpf 2013). For this reason, the monitoring of landslides is considered a powerful weapon in the hands of geologist and engineers for the assessment and control of the stability of a slope and for the prediction of its future evolution. As a result, landslide monitoring has stimulated

manufacturers to design suitable new instruments and service providers for the development of new system architectures (Mazzanti and Pezzetti 2013).

The monitoring of a landslide is defined as the periodical data acquisition and analysis of a series of observations over time in order to extract information on spatial and temporal changes of relevant parameters within a landslide area (Stumpf 2013). At present, the monitoring of a landslide is not only scientifically useful, but also beneficial for the assessment of landslide hazards and risk (Wieczorek and Snyder 2009). In order to observe the evolution of the landslide by analyzing the kinematics of the movement, very often the measurement of the superficial displacements (i.e., deformation mapping or monitoring of a landslide) is carried out (Gili et al. 2000). However, a large variety of geomorphological, geological, geomechanical, and geotechnical conditions affect the identification of the most suitable parameters and of the best instrumental solutions (Mazzanti and Pezzetti 2013). Thus, over the past 20 years, different technologies and techniques have been used in landslide science, ranging from inexpensive short-term solutions to costlier long-term monitoring programs. The aim is to achieve better knowledge of earth phenomena, to reduce landslide risk, and to improve disaster mitigation and preparedness capability (Savvaidis 2003; Mazzanti 2012; Mazzanti and Pezzetti 2013; Eker and Aydın 2014; Scaioni 2015). These technologies/techniques can be classified as follows: (1) ground-based geodetic techniques, e.g., electronic theodolites, electronic distance measurement, dual-frequency instruments, three-dimensional positioning systems, automatic levels, digital levels, zenith angle methods, and total station instruments; (2) satellite-based geodetic techniques, e.g., global positioning systems (GPS) and real-time kinematics (RTK) GPS); (3) geotechnical techniques, e.g., extensometers, inclinometers, piezometers, strain meters, pressure cells, geophones, tilt meters, and crack meters; and (4) remote sensing techniques, e.g., high-resolution optical satellite imagery, satellite interferometric synthetic-aperture radar (InSAR), ground-based InSAR, airborne and terrestrial laser scanners, unmanned aerial vehicles (UAVs), aerial photographs, and terrestrial photogrammetry (Savvaidis 2003).

Lately, among the techniques mentioned above, geodetic techniques, and in particular GPS, are commonly being used with high accuracy for monitoring ground motion (Brückl et al. 2006). However, geodetic techniques can require access to a field with dangerous topography, and thus could be unsafe for the operator. In addition, these techniques may be time consuming and costly due to their dependency on the huge spatiotemporal information density of larger-sized case areas (Dewitte et al. 2008). In addition, because these techniques largely employ point-based instruments of measurement, the density of points is also relatively low (Abellán et al. 2010). In order to remove these limitations, remote sensing techniques are used as alternative and/or complementary methods of gathering information about the distribution and kinematics of landslides as well as their conditioning factors. However, since remote sensing technologies are not designed specifically for landslide observation, they require adaptation and validation in order to exploit their capabilities for such research and operational applications (Stumpf 2013).

Orbital and suborbital-based remote sensing systems are the primary platforms for observation of the Earth (Zhou and Zang 2007; Xiang and Tian 2011). However, small UAVs continue progressively to gain importance in remote sensing applications in scientific and practical areas as an alternative remote sensing platform (Wallace et al. 2012; Nebiker et al. 2008) and/or a new photogrammetric measurement tool (Eisenbeiss 2009) because detailed topographic surveys are the key to and a prerequisite for many studies in Earth science (Hackney and Clayton 2015). This technology is commonly referred to as a drone, unmanned/uninhabited air/aerial vehicle (UAV), or remotely piloted aircraft (RPA) (Ambrosia et al. 2003; Watts et al. 2012). As the names suggest, this technology employs a powered aerial vehicle without a human operator inside (Dunford et al. 2009; Bendea et al. 2008). The term "UAV," which is more common in the literature, covers all vehicles flying in the air with no person on board having the capability of controlling the aircraft (Eisenbeiss 2004). In general, two types of mini-UAVs are currently available: multicopters and fixed-wing UAVs (Anders et al. 2013). Due to their ability to achieve very high resolution in acquired images, low-altitude mini-UAVs are used to carry lightweight instruments such as consumer digital cameras or combinations of imaging systems covering the visible (e.g., webcams) to the thermal spectrum (e.g., temperature or moisture sensors) with multi- or hyperspectral sampling (e.g., hyperspectral cameras), miniature radar, passive microwave radiometers, and light detection and ranging (LIDAR) sensors (Sugiura et al. 2007; Everaerts 2008; Colomina and

Molina 2014). Multicopters are more suitable for carrying various payloads due to the increased number of rotors, resulting in the possibility of installing more advanced sensing systems (Anders et al. 2013).

Recently, the number of scientific studies on UAV-based remote sensing of landslides has increased (Niethammer et al. 2009; Carvajal et al. 2011; Lucieer et al. 2014; Peterman 2015; Turner et al. 2015; Vrublová et al. 2015; Lindner et al. 2016; Tanteri et al. 2017; Mateos et al. 2017; Peternal et al. 2017). The current literature shows that UAV-based landslide monitoring is a viable method (Turner et al. 2015). The combination of UAV-based aerial photos and structure from motion (SfM) software provides an efficient, low-cost, and rapid framework for the remote sensing and monitoring of dynamic natural environments (Clapuyt et al. 2016). In landslide assessment studies, a time series of high-resolution images is used to create digital elevation models (DEMs) and orthophotos by applying SfM techniques. The SfM is a photogrammetric method for creating 3D (three-dimensional) models of a feature or topography from overlapping 2D photos taken from many locations and orientations in order to reconstruct the photographed scene (Shervais 2015). Although SfM has existed in various forms since 1979 (Ullman 1979), it only began to be commonly applied in the early 2000s (Snavely et al. 2008). The SfM process starts by acquiring photographs with sufficient overlap (e.g., 80–90%) from multiple positions and/or angles (Lucieer et al. 2014).

A variety of technique for quantifying topographic changes (i.e., elevation and/or volumetric change) between successive topographic surveys can be used in landslide investigation and monitoring. This involves the possibility of acquiring 3D information of the terrain generated from different data sources such as airborne laser scanning (ALS), aerial stereo-photographs, UAV-based digital images, etc. with high accuracy and high spatial resolution (Jabodeyoff et al. 2012). These techniques are referred to as distance measurement techniques/methods and can be classified as follows: (1) DEM of difference (DoD), (2) direct cloud-to-cloud comparison with closest point technique, and (3) cloud-to-mesh (or model) comparison (Lague et al. 2013). The DoD, one of the most straightforward methods, involves the subtraction of an earlier elevation model from a later elevation model (Hsieh et al. 2016). This subtraction is made on a pixel-by-pixel basis, which provides measured values of vertical distance

(Lague et al. 2013). One of the latest methods used for direct point cloud comparison is the Multiscale Model-to-Model Cloud Comparison (M3C2), introduced by Lague et al. (2013). The M3C2 algorithm works as a plug-in under CloudCompare 3D processing software. This algorithm can also be used for landslide monitoring (Warrick et al. 2017).

In the present study, the Gallenzerkogel landslide (Ybbs, Lower Austria) was monitored using UAV data as well as LIDAR data. Three UAV flights were carried out, and the SfM algorithm was applied to create high-resolution DEMs, orthophotos, and point clouds. The DoD and M3C2 algorithm were used to analyze landslide behavior.

Material and methods

Study area and available datasets

Gallenzerkogel landslide, located in the municipality of Hollenstein (Ybbs, Lower Austria), was selected as the study area (Fig. 1). The upper left coordinates are − 117,839.42, 295,545.08, and the bottom right coordinates are − 117,421.13, 295,284.58 in MGI Austria GK M31. The landslide area, covering 7.46 ha, is located between 760 m and 495 m a.s.l., and slope gradients reaching up to 70% can be seen. Former events in the area have also been reported (Schweigl 2014). The oldest known documented event was in 1899, with 7500 m^3 of displacement. Furthermore, in 2014, it was reactivated with a total of ca. 2000 m^3 of displacement (Hubl et al. 2016). In the present study, 2009 LIDAR data representing the prefailure topography (1 m of resolution) were obtained as both a digital surface model (DSM) and a digital terrain model (DTM) (Fig. 2).

UAV-based image acquisition

The main steps of the workflow of the UAV-based image acquisition can be categorized as follows: (1) off-site preparation, (2) on-site preparation and image acquisition, and (3) postprocessing (Lindner et al. 2016). Off-site preparation included several prerequisites that had to be determined before moving on-site, such as weather conditions and topography of the area of interest. The optimal weather conditions for UAV-based surveying of a landslide are a cloudy sky, but with no rain, as it has a negative impact on UAV electronics
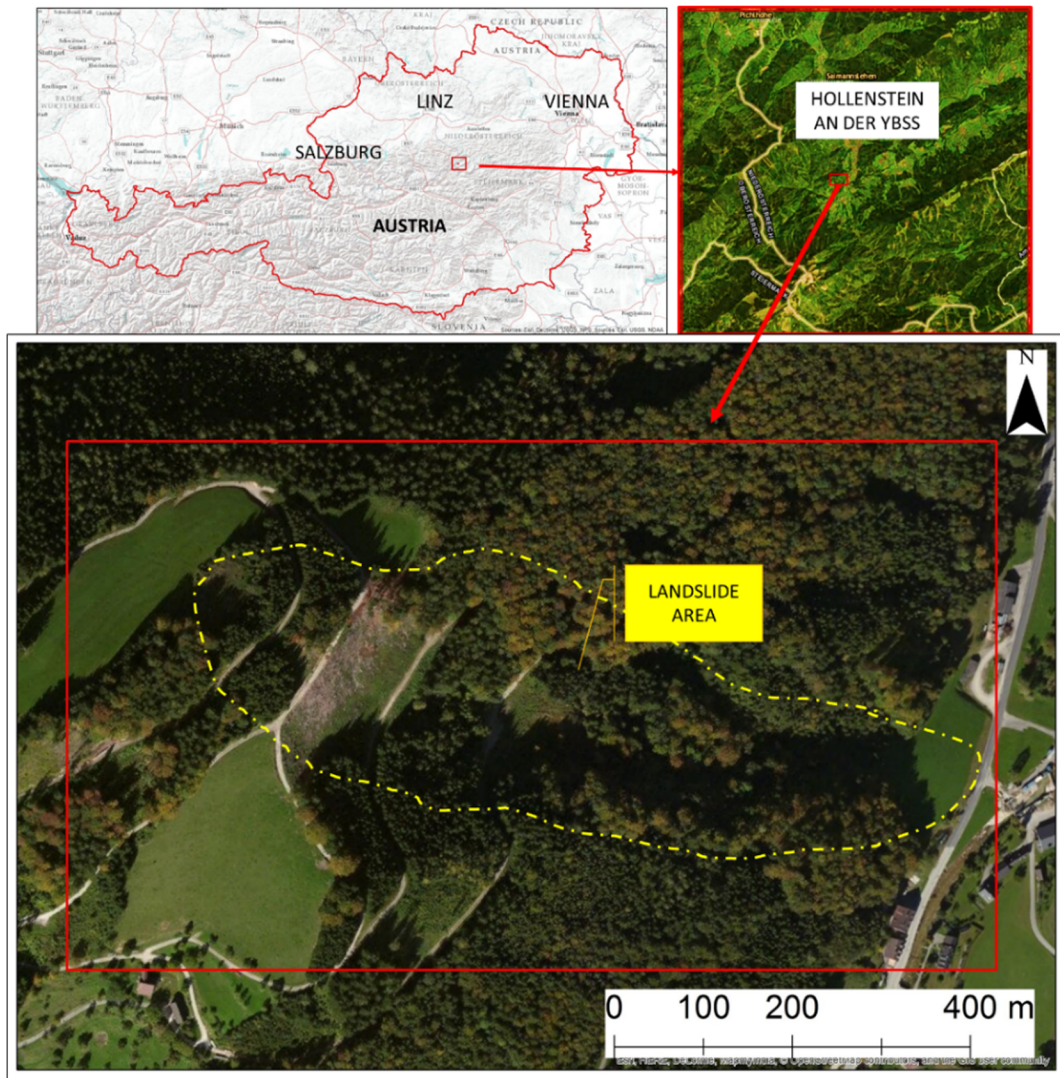
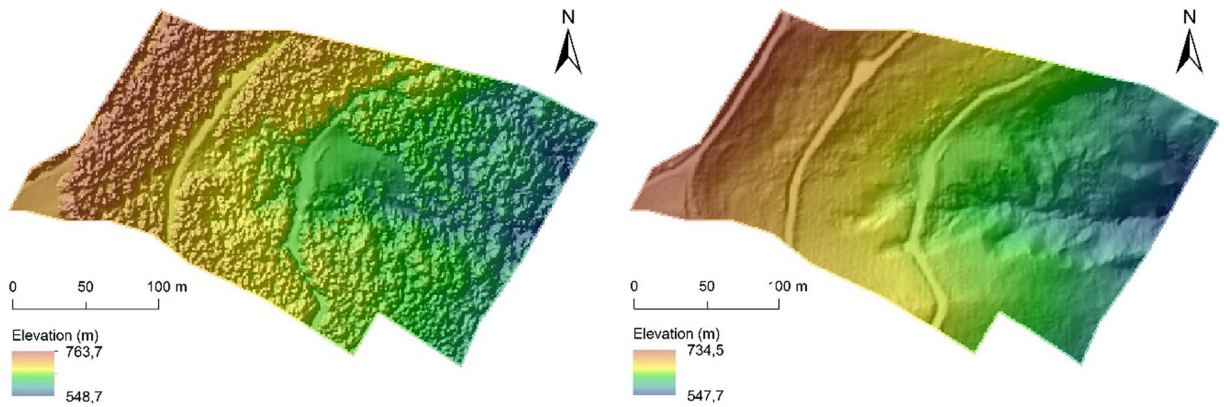**Fig. 1** Location map of Gallenzerkogel landslide

Fig. 2 LIDAR-DSM (left) and LIDAR-DTM (right)

and on the quality of images, and no wind, as it has a negative impact on the precision of the global navigation satellite system (GNSS) route and the sharpness of the image. The topography of the area of interest was assessed roughly by using Google Earth in order to determine the highest and lowest points as well as the average slope because these are important for generating the GNSS route for automatic flights. A regular flight with all the necessary information will result in a successful survey with regard to the quality of the images and with adequately overlapped rates (> 90% forward overlapping and > 70 side overlapping).

The on-site preparation and image acquisition stage included the flights and field work. The ground control points (GCPs) required for image processing were surveyed with subcentimeter accuracy (less than 5 mm) by using Real-Time Kinematic-Global Positioning System (RTK-GPS). The GCPs are shown in Table 1. Each GCP is clearly visible in the acquired photograph (Fig. 3). This GCP information is necessary for image rectification and image geocoding.

For the UAV-based aerial survey of Gallenzerkogel landslide, three flight missions were carried out (Table 1). The UAV system used for the present study (Fig. 4), a rotary-wing mini-octocopter (i.e., multicopter UAV), the ARF MikroKopter OktoXL having the dimensions of 73 × 73 × 50 cm and weighing about 4.9 kg (including camera and batteries), was also used by Lindner et al. (2016). The UAV was equipped with GNSS, which records spatial positions at 1-s intervals for the X and Y positioning onto an SD card, and a barometer, which determines the height above ground level (AGL). These spatial positions were required for the subsequent processing steps. The flight control software MikroKopterTool was used to create a raster of GNSS waypoints in the air, followed by the UAV with user-controlled velocity and AGL height.

All flight missions were automatically controlled by the defined GNSS waypoint raster, and manual intervention was required only for starting and landing the multicopter. Flight duration depended on the battery package and thus lasted no longer than 15 min for all missions in order to avoid a crash. The mean altitude of the flight missions was set to less than 60 m AGL. A Canon EOS 650D DSLR camera with a resolution of 18 megapixels was carried by the UAV to take all images. In order to acquire a sufficient number of images for photogrammetric analysis, the camera was adjusted to be triggered automatically at a constant time interval of 2 s, independent of its position and orientation in the space. Some key figures of the flight missions are in given in Table 1.

Postprocessing included the georeferencing of all obtained images with the GNSS log from the multicopter and also by means of the GCPs using Agisoft Photoscan. For each flight mission, point clouds, DEMs, and orthophotos were generated to use for further analysis in GIS software (ESRI ArcGIS) and cloud processing software (CloudCompare) in order to evaluate the landslide event.

Point cloud, DEM, and orthophoto generation

In the present study, the SfM algorithm was applied to generate point clouds, DEMs, and orthophotos, using Agisoft Photoscan Professional version 1.1.6. This procedure is included in the postprocessing stage of the UAV aerial survey. The workflow of the SfM algorithm in Photoscan is described as (1) image preparation, (2) image matching and bundle block adjustment, (3) dense geometry reconstruction and inclusion of GCPs, and (4) texture mapping and export of DEMs and orthophotos (Lucieer et al. 2014). In the image preparation step, the GPS information registered on board the multicopter

Table 1 Some key figures of flight missions

Date	Number of flight	Number of images	Average flight height (m AGL)	Focal length (mm)	ISO	Shutter speed	GSD (cm/px)	Area covered (Ha)	Number of GCP
21.04.2015	3	396	40.69	20	200	1/400	0.896	6.10	9
04.11.2015	1	116	39.27	24	400	1/320	0.721	5.13	9
04.04.2016	1	94	41.38	24	200	1/400	0.759	5.00	8

Fig. 3 Depiction of GCP surveyed with RTK-GPS, which is well visible in UAV image
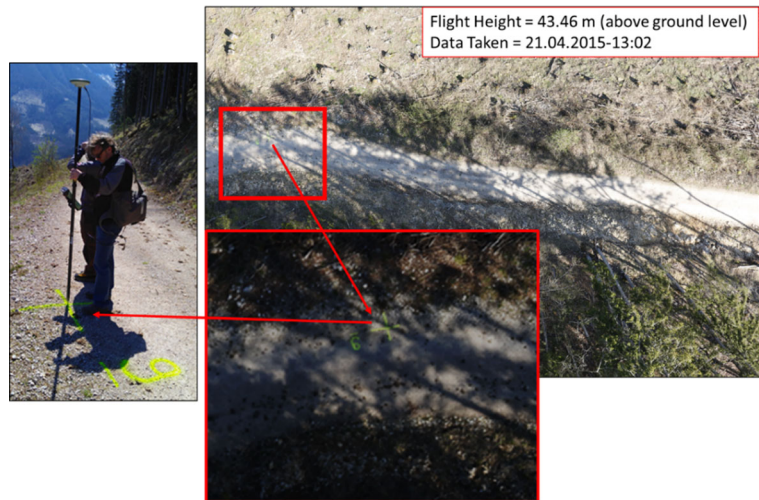
(i.e., photograph location from the UAV flight path) was linked to all UAV images obtained using the time setting of the digital camera. In this way, UAV-GPS coordinates were written to the corresponding JPEG-EXIF headers. This process is also called "geotagging." Following the importation of the selected geotagged UAV images in Photoscan, image alignment was carried out based on GPS information stored in the JPEG-EXIF headers. Photoscan automatically positions the images and matches features within the UAV images that overlap. Bundle block adjustment was then carried out and outliers were deleted from the sparse point cloud to avoid reconstruction errors. In the dense geometry reconstruction and inclusion of the GCPs stage, a dense 3D geometry was built using a "height field" as well as other parameters defined in Photoscan. The GPS markers (i.e., field-measured GPS coordinates of the GCPs) were then defined in order to recalculate and fine-tune the bundle adjustment with the estimated accuracy. Markers were used to optimize camera positions and orientation data.

Based on the updated bundle adjustment, the dense 3D geometry was recomputed to obtain better model reconstruction results. Following recomputation of the dense 3D geometry based on the markers, texture mapping of the 3D model was carried out based on the original UAV images. After the texture mapping, DEMs (in GeoTiff) and orthophoto mosaics were exported for analysis via GIS software. As a part of the bundle adjustment and model generation process, the accuracy of all 3D models was assessed based on the XYZ residuals for the GCPs that were calculated by Agisoft. In addition, Agisoft allows the users to export point clouds generated for analysis in other cloud processing software.

UAV-based monitoring of Gallenzerkogel landslide

In the present study, the DoD was applied by subtracting the DEM obtained from the first flight of the UAV from the LIDAR-DEM because the LIDAR-DEM, representing the prefailure topography, was obtained as

Fig. 4 MikroKopter OktoXL UAV (left) and remote controller and ground control set (right)

both a DTM and a DSM. Here, before the DoD was applied, the UAV-DSM obtained from the first UAV flight was resampled as 1 m, because the LIDAR-DEM had a 1 m resolution. Following the resampling, in order to validate the alignment of these two DSMs (LIDAR and UAV), the root mean square error (RMSE) was calculated by using 770 points located over places without vegetation cover outside the active landslide area. Lower value indicates good agreement between two datasets. A similar comparison approach had been employed in several related studies in the literature (Lucieer et al. 2014; Immerzeel et al. 2014; Turner et al. 2015). In addition to the vertical difference obtained by the DoD application, volumetric changes were taken from the difference map in a way similar to that employed by Turner et al. (2015).

In this study, cloud-to-cloud distance computation between the first and second UAV flights was carried out using the M3C2 plug-in of CloudCompare 3D processing software in order to monitor landslide activity during the period following the first UAV flight. This comparison was made because of the density of the vegetation surrounding the landslide area. However, because of the ongoing landslide control/stabilization work over the landslide area, the third UAV flight was not used to monitor landslide activity. The M3C2 algorithm (see Lague et al. 2013 for detailed explanation) enables the detection of changes in complex topography directly on point clouds, without meshing or gridding (Esposito et al. 2017). The required parameters in computing the distance between two point clouds by using the M3C2 algorithm include (1) definition of the reference cloud and comparison cloud; (2) definition of the core points; (3) definition of the normal scale (D), the projection scale (d), and the cylinder depth; and (4) definition of the registration error (Esposito et al. 2017). To this aim, the first UAV flight was set as the reference and the second UAV flight was set as the compared cloud. For the cloud-to-cloud comparison, point clouds generated by Agisoft PhotoScan were exported as a text file (.txt). The parameters D and d were chosen based on the suggestions reported by Lague et al. (2013). The normal-scale parameter was set as the fixed value of 5 m for this study, being specifically more than 25 times greater than the average roughness (0.17 m) because no corresponding elements could be identified between surveys. The projection scale was set at 2 m as it would be suitable for point distance computation with the average point density of

5.2 pts./m^2. This is more than the minimum of four points requested by the M3C2 algorithm (Esposito et al. 2017). The cylinder depth was set at 2 m for the points representing the vegetation. Both clouds were subsampled at 50-cm minimum point spacing, and the first UAV flight data (i.e., the reference cloud) was used for the core points. In addition, the registration error (reg) was calculated by using Eq. 1 (Esposito et al. 2017).

$$reg = \sqrt{\left(RMSE_{ref}\right)^2 + \left(RMSE_{comp}\right)^2} \qquad (1)$$

where RMSE is the root mean square error of the models calculated from the GCPs used in Agisoft Photoscan. In this study, the registration error was calculated as 0.063 m. The outputs of the M3C2 algorithm are the distance to the closest corresponding point, significant change, and distance uncertainty. The distance uncertainty is the 95% level of detection ($LOD_{95\%}$) and was calculated by the M3C2 algorithm using Eq. 2 (Borradaile 2003).

$$LOD_{95\%} = \pm 1.96 \left(\sqrt{\frac{\sigma_1(d)^2}{n_1} + \frac{\sigma_2(d)^2}{n_2}} + reg \right) \qquad (2)$$

where d is the projection scale and $\sigma_1(d)^2$ and $\sigma_2(d)^2$ are the local roughness of the point clouds n_1 and n_2. In this study, distance uncertainty values of higher than 15 cm and nonsignificant changes were removed and the remaining points were used to obtain the landslide deformations.

Results and discussion

### Results of UAV flights and SfM processing

In the present study, three flight missions with a UAV (ARF MikroKopter OktoXL) were carried out over the landslide area. There was an interval of 197 days between the first and second UAV flights, and 152 days between the second and third UAV flights used to take the images. The standards of the camera used for this study (Canon EOS 650D DSLR with resolution of 18 megapixels) were sufficient for data acquisition in daylight. Same system was also used successfully by Lindner et al. (2016). All images had a ground sampling distance (GSD) of less than of 1 cm. All UAV flights lasted about 10 min, and all field work covering the

entire on-site preparation and image acquisition step of the UAV-based image acquisition was completed in less than 2 h except for the driving time to the study area. This duration is quite short when compared to traditional field surveys. All orthophotos generated using Agisoft Photoscan are given in Fig. 5. All DEMs and orthophotos were produced at a resolution of 10 cm, and all models were generated with an average of 4 cm RMSE according to the GCPs. The RMSE values for data from the first, second, and third flights were 0.06, 0.02, and 0.04 m, respectively. These values are comparable with Turner et al. (2015) and Lindner et al. (2016). In total, 396 images for the first UAV flight mission, 116 images for second, and 94 images for third were taken to generate the models. As the highest number of images were taken during the first flight, the best-quality orthophotos were obtained. The decrease in the number of overlapping images resulted from the decrease in the number of images taken by the latter two flights, as the vegetation density around the slide area (i.e., the most active part of the slope), generated models having more noise. However, even though there was some noise, all data

could be used for the monitoring of the landslide because one of the outputs obtained by the SfM algorithm was a high-density point cloud. All point clouds generated had more than ten million points, resulting in a point density of more than 150 pts./m^2.

Results of monitoring of Gallenzerkogel landslide

The UAV-based DSMs, orthophotos, point clouds, and LIDAR-DEMs (obtained as DTMs and DSMs) were used for the monitoring of the Gallenzerkogel landslide. The LIDAR-DEM (resolution of 1 m) from 2009 represented the prelandslide topography. The monitoring of the landslide was first carried out by applying DoD. Before applying DoD, the RMSE of LIDAR-DEM and first UAV-DEM was calculated by using 770 points located over places outside the active landslide area without vegetation cover. The RMSE value was determined as 0.2 m. The elevation distribution of selected points is depicted as a graph in Fig. 6. According to this graph, the UAV-DSM data is quite compatible with the LIDAR-DTM data. The pixels having values in
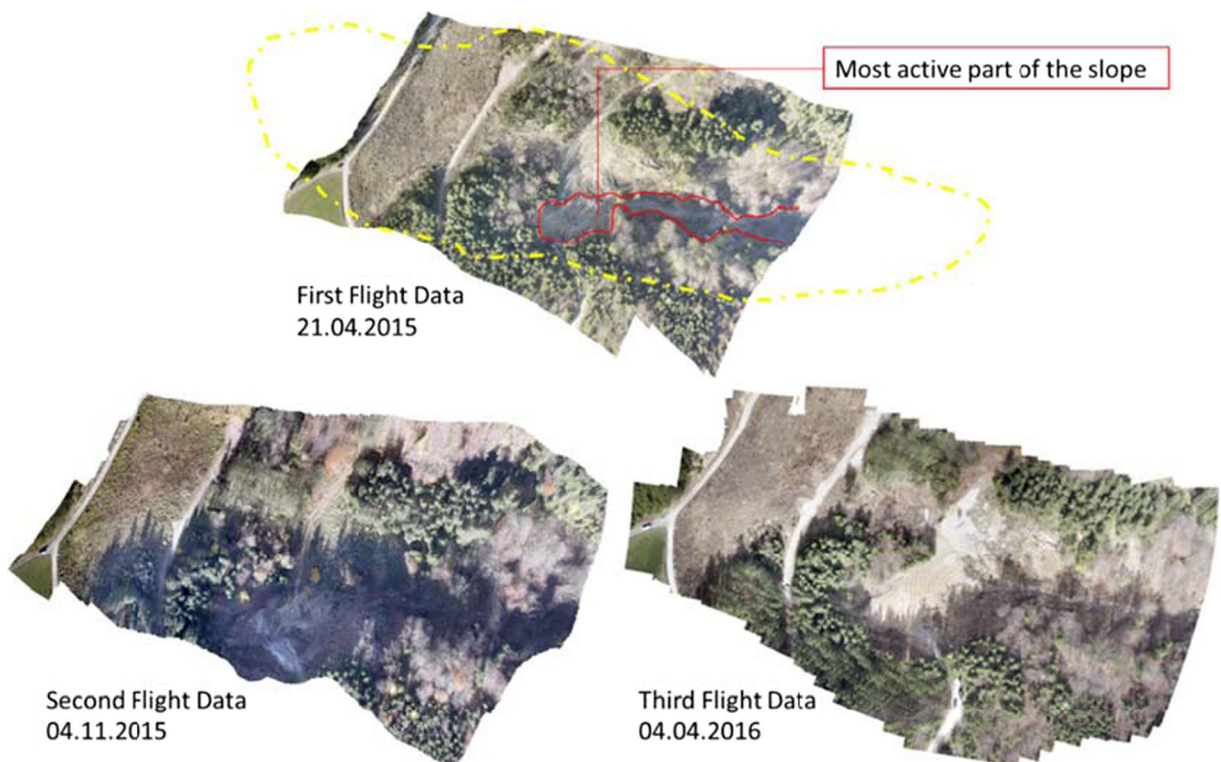
**Fig. 5** Orthophotos (10 cm) generated from UAV images of Gallenzerkogel landslide

Fig. 6 Elevation distribution graph of selected points from outside of the landslide
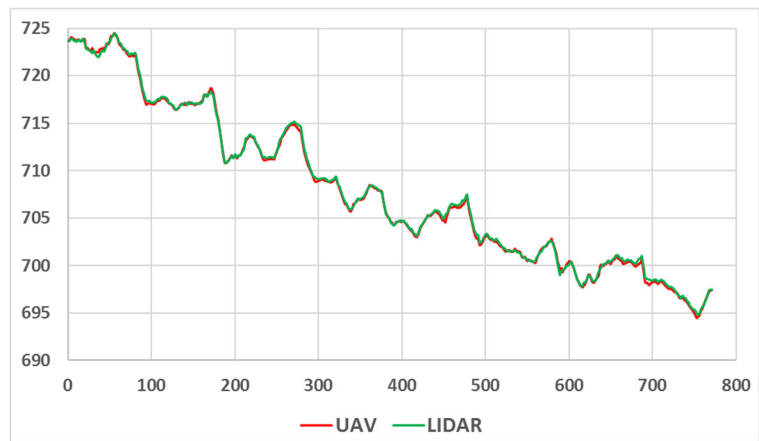
the range of ± 0.2 m were eliminated from the deformation map obtained by DoD. First, in order to observe the change in vegetation between the LIDAR-DSM and the first UAV-DSM data, the differences that were reclassified as less than − 15 m (selected depending on field observations) were obtained by the DoD method (Fig. 7). This map shows both the trees that were destroyed by the landslide and the trees that were removed due to the landslide in the area. In addition, in order to obtain landslide deformations, the DoD was applied by subtracting the first UAV-DSM from the LIDAR-DTM. Because the UAV-DSM data included vegetation cover, the differences of greater than 2 m were eliminated. According to the deformation map, the difference was between − 6.6 and 2 m (Fig. 7). Over the landslide area, a total of 4380.1 m³ of the slope material was eroded, while
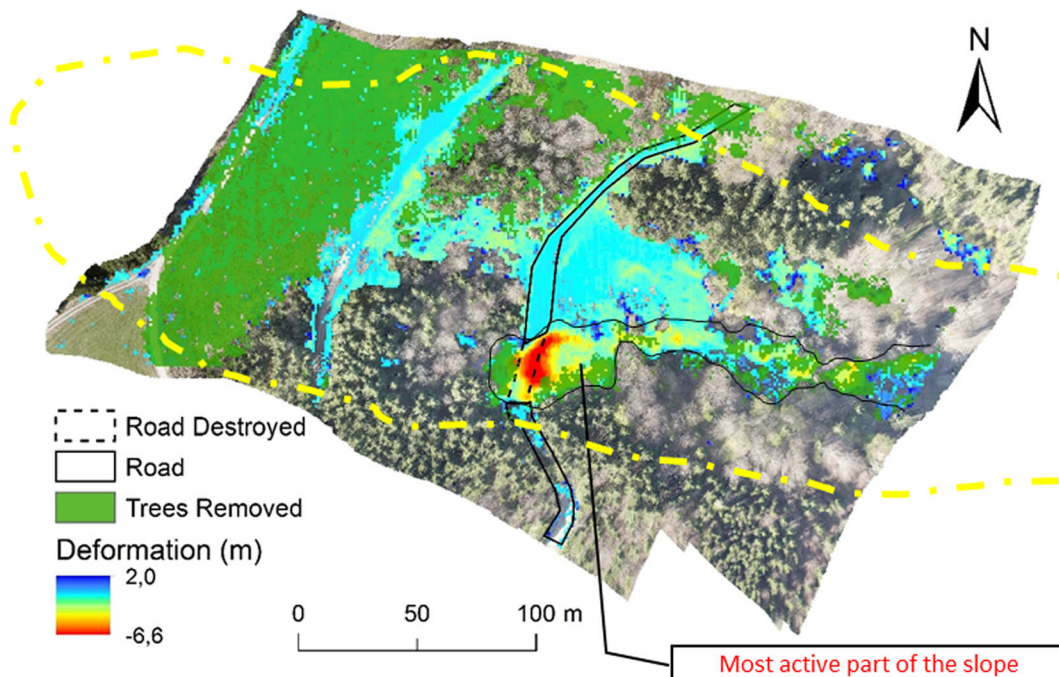

Fig. 7 Landslide deformations mapped between first UAV and 2009 LIDAR. This map is combination of difference of UAV-DSM and LIDAR-DSM and difference of UAV-DSM and LIDAR-DTM

297.4 m^3 of the material had accumulated within the most active part of the slope. In addition, 688.3 m^3 of the total eroded material had belonged to the road destroyed by the landslide.

In the present study, in order to monitor landslide activity during the period following the first UAV flight, a cloud-to-cloud comparison was carried out using the M3C2 algorithm. The cloud-to-cloud comparison of the first and second UAV flight data was applied because when the UAV meshes were generated, the vegetation surrounding the landslide area caused more noise. The outputs of the M3C2 algorithm are given in Fig. 8. The colors in the legend of Fig. 8 represent the attributes for

each piece of information (significant change at the top, distance uncertainty in the middle, and M3C2 distance at the bottom). The M3C2 distance, after eliminating both the distance uncertainty values of higher than 15 cm and the nonsignificant changes, was determined as − 2.5–2.5 m. Related uncertainty values ranged from 12.3 to 15 cm, with a mean value of 13.4 cm and a standard deviation of 7.4 mm (Fig. 8).

In the present study, neither DoD nor M3C2 methods could be used with the third flight data to monitor landslide activity. This was due to the landslide control/stabilization work, which had markedly increased following the date of the second flight, and the
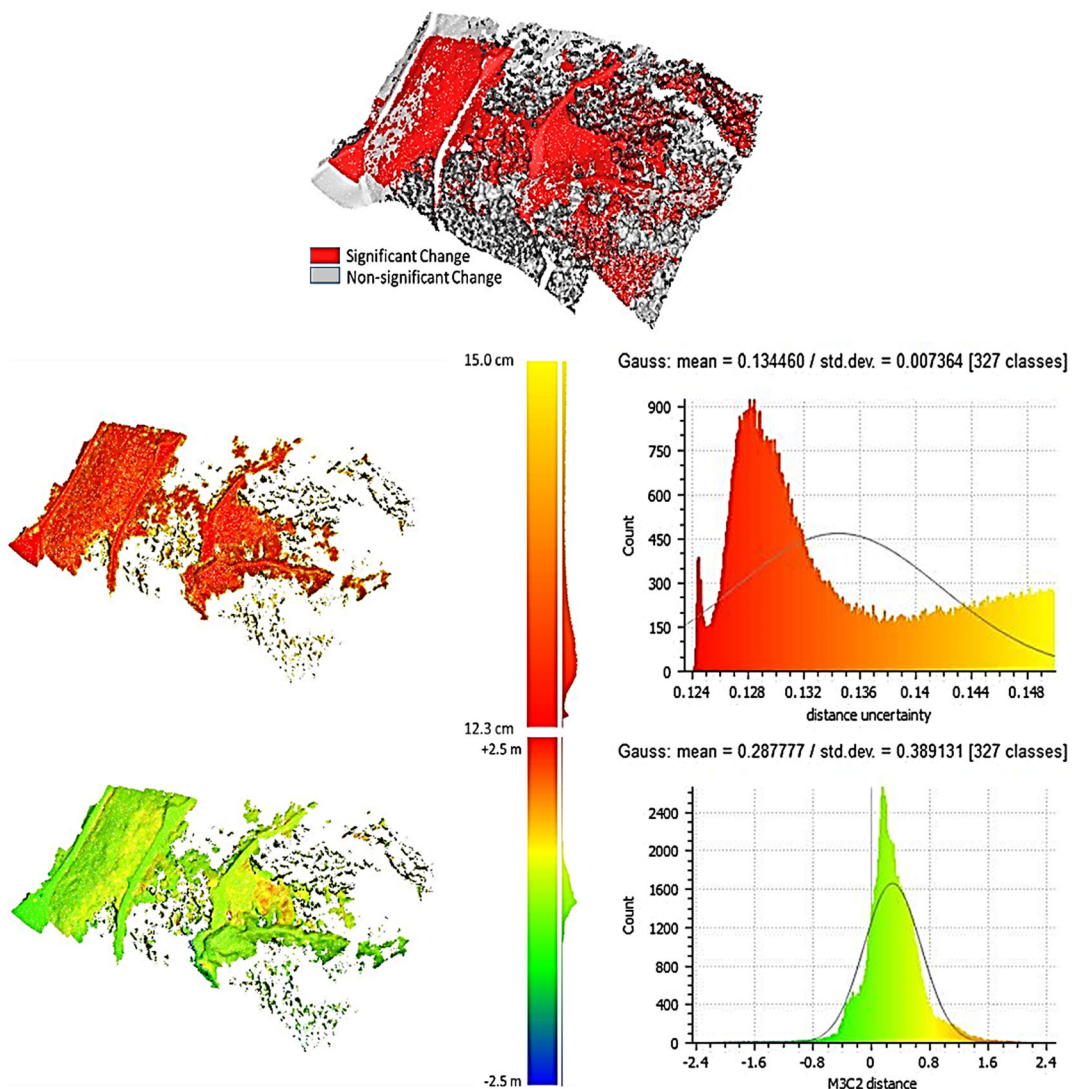
Fig. 8 Outputs of cloud-to-cloud comparison (M3C2) of first and second UAV flights. Significant change (top), distance uncertainty (middle), and M3C2 distance (bottom)
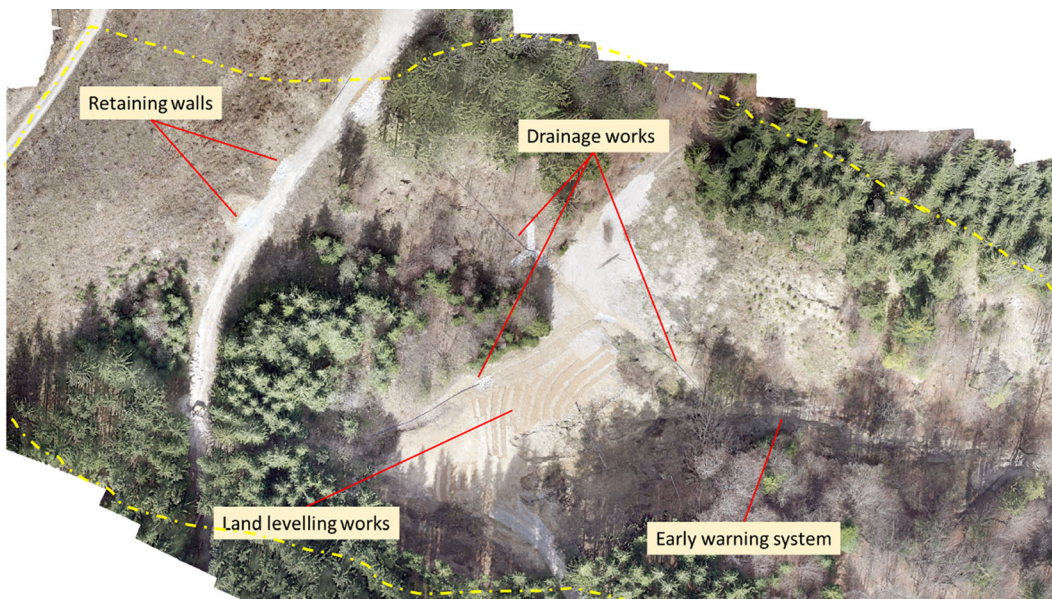
Fig. 9 Landslide control works made over Gallenzerkogel landslide (orthophoto of the third UAV flight)

resulting excavation and replacement of the earth mate-
rial in the study area. Thus, the landslide control/
stabilization work had considerably changed the topog-
raphy data between the second and third flights. How-
ever, the high-resolution orthophotos enabled the visual
monitoring of the control/stabilization work in the area
(Fig. 9).

Conclusions

In this study, a case application of UAV-based photo-
grammetry was carried out for the Gallenzerkogel
(Lower Austria) landslide, via three flights conducted
after the landslide event and LIDAR data representing
the prefailure topography. The presence of the LIDAR
data of the area enabled the LIDAR and UAV data to be
combined in the study. A standard digital camera was
used to collect RGB (true color) images for all UAV
flights. The SfM was used to obtain DEMs,
orthophotos, and point clouds from hundreds of over-
lapping images. All SfM outputs were successfully used
for the monitoring of the landslide. The UAV-DEMs and
orthophotos show great potential for analysis of land-
slide behavior.

One of the important advantages of UAVs is that they
can be utilized at almost any moment in time. This
means that using UAVs is a flexible, quick, and effective
method for the acquisition of multitemporal data. In the

study, for the three flights over Gallenzerkogel land-
slide, taking images via UAV over an area of about
5 ha took 10 min. Another advantage of UAV-based
photogrammetric measurement is the completeness of
the data. All monitoring was made for the landslide as a
whole, not just for random points of interest. In addition,
UAVs provide a level of detail that could not be obtained
by traditional methods. All images had GSD values of
less than 1 cm, while the DEMs and orthophotos pro-
vided high resolutions (i.e., in centimeters) and the point
clouds had very high densities (i.e., higher than 150 pts./
m^2). For all flights, only nine GCPs could be surveyed
in the field work. Conducting surveys of GCPs in the
field was a challenging task and in most cases, up to half
of the time spent in the UAV missions was due to GCP
placement. Moreover, this task can be more challenging
in hazardous areas such as landslides. In addition, man-
ual placement of GCPs on the images during the exterior
orientation process in Agisoft Photoscan Professional
may introduce a further source of error.

In this study, both DoD and M3C2 were used for
analysis of landslide deformations. According to DoD, a
total of 4380.1 m^3 of the slope material was eroded,
while 297.4 m^3 of the material had accumulated within
the most active part of the slope. In addition, 688.3 m^3 of
the total eroded material had belonged to the road
destroyed by the landslide. The M3C2 algorithm proved
to be suitable and satisfactorily accomplished accurate
change detection results when compared to the most

common DoD. The M3C2 algorithm, a modern methodology for change detection analysis, enabled the detection of changes in complex topography directly on point clouds, without meshing or gridding. Because the vegetation surrounding the landslide area caused more noise in generating meshes, the M3C2 algorithm was used as cloud to cloud comparison. The outputs of M3C2 algorithm are distance uncertainty and nonsignificant change between two series of data. Only deformations caused by landslide activity could map by eliminating both the distance uncertainty values and the nonsignificant changes. Since the landslide control/ stabilization work had considerably changed the topography data between the second and third flights, neither DoD nor M3C2 methods could be used with the third flight data. But ongoing control/stabilization works were able to be monitored with high-resolution orthophotos.

References

Abellán, A., Calvet, J., Vilaplana, J. M., & Blanchard, J. (2010). Detection and spatial prediction of rockfalls by means of terrestrial laser scanner monitoring. *Geomorphology, 119*(3–4), 162–171. https://doi.org/10.1016/j.geomorph.2010.03.016.

Ambrosia, V. G., Wegener, S. S., Sullivan, D. V., Buechel, S. W., Dunagan, S. E., Brass, J. A., Stoneburner, J., & Schoenung, S. M. (2003). Demonstrating UAV-acquired real-time thermal data over fires. *Photogrammetric Engineering & Remote Sensing, 69*(4), 391–402. https://doi.org/10.14358/PERS.69.4.391.

Anders, N., Masselink, R., Keessra, S., Suomalainen, J. (2013). High-res digital surface modeling using fixed-wing UAV-based photogrammetry. In Proceedings of the Geomorphometry, Nanjing, China, 16–20 October 2013.

Bendea, H., Boccardo, P., Dequal, S., Tonolo, F. G., Marenchino, D., & Piras, M. (2008). Low cost UAV for post-disaster assessment. Proceeding of the The International Archives of

the Photogrammetry. *Remote Sensing and Spatial Information Sciences, XXXVII*(Part B1. Beijing), 1373–1379.

Borradaile, G. J. (2003). *Statistics of earth science data: Their distribution in space, time, and orientation* (Vol. XXVII, p. 351). Berlin Heidelberg: Springer-Verlag. https://doi.org/10.1007/978-3-662-05223-5.

Brückl, E., Brunner, F. K., & Kraus, K. (2006). Kinematics of a deep-seated landslide derived from photogrammetric, GPS and geophysical data. *Engineering Geology, 88*(3–4), 149–159. https://doi.org/10.1016/j.enggeo.2006.09.004.

Carvajal, F., Agüera, F., & Pérez, M. (2011). Surveying a landslide in a road embankment using unmanned aerial vehicle photogrammetry. *The International Archives of the Photogrammetry, Remote Sensing and Spatial Information Sciences, XXXVIII*(Part 1/C22), 201–206.

Clapuyt, F., Vanacker, V., & Oost, K. V. (2016). Reproducibility of UAV-based earth topography reconstructions based on structure-from-motion algorithms. *Geomorphology, 260*, 4–15. https://doi.org/10.1016/j.geomorph.2015.05.011.

Colomina, I., & Molina, P. (2014). Unmanned aerial systems for photogrammetry and remote sensing: A review. *ISPRS Journal of Photogrammetry and Remote Sensing, 92*, 79–97. https://doi.org/10.1016/j.isprsjprs.2014.02.013.

Dewitte, O., Jasselette, J. C., Cornet, Y., Van Den Eeckhaut, M., Collignon, A., Poesen, J., & Demoulin, A. (2008). Tracking landslide displacements by multi-temporal DTMs: A combined aerial stereophotogrammetric and LIDAR approach in western Belgium. *Engineering Geology, 99*(1-2), 11–22. https://doi.org/10.1016/j.enggeo.2008.02.006.

Dunford, R., Michel, K., Gagnage, M., Piégay, H., & Trémelo, M. L. (2009). Potential and constraints of unmanned aerial vehicle technology for the characterization of Mediterranean riparian forest. *International Journal of Remote Sensing, 30*(19), 4915–4935. https://doi.org/10.1080/01431160903023025.

Eisenbeiss, H. (2004). A mini unmanned aerial vehicle (UAV): System overview and image acquisition. *International Archives of Photogrammetry. Remote Sensing and Spatial Information Sciences, 36*(5/W1), 7.

Eisenbeiss, H. (2009). UAV photogrammetry. Ph.D. Thesis, Institute of Geodesy and Photogrammetry, ETH Zurich, Zurich, Switzerland, 2009; p. 235.

Eker, R., & Aydın, A. (2014). Assessment of forest road conditions in terms of landslide susceptibility: A case study in Yığılca Forest Directorate (Turkey). *Turkish Journal of Agriculture and Forestry, 38*, 281–290. https://doi.org/10.3906/tar-1303-12.

Esposito, G., Mastroroceo, G., Salvini, R., Oliveti, M., & Starita, P. (2017). Application of UAV photogrammetry for the multi-temporal estimation of surface extent and volumetric excavation in the Sa Pigada Bianca open-pit mine, Sardinia, Italy. *Environment and Earth Science, 76*(3), 103. https://doi.org/10.1007/s12665-017-6409-z.

Evaerts, J. (2008). The use of unmanned aerial vehicles (uavs) for remote sensing and mapping. *Proceeding of the The International Archives of the Photogrammetry, Remote Sensing and Spatial Information Sciences, XXXVII*(Part B1. Beijing), 1187–1191.

Gili, J. A., Corominas, J., & Rius, J. (2000). Using global positioning system techniques in landslide monitoring.

Engineering Geology, 55(3), 167–192. https://doi.org/10.1016/S0013-7952(99)00127-1.

Hackney, C., Clayton, A.I. (2015). Unmanned aerial vehicles (UAVs) and their application in geomorphic mapping. In L. Clarke & J. Nields (Eds.), Geomorphological Techniques, British Society for Geomorphology, pp 1–12.

Hsieh, Y.C., Chan, Y., Hu, J. (2016). Digital elevation model differencing and error estimation from multiple sources: A case study from the Meiyuan Shan landslide in Taiwan. Remote Sens., 8, 199.

Hübl, J., Beck, M., Zöchling, M., Moser, M., Kienberger, C., Jenner, A., Forstlechner, D. (2016). Ereignisdokumentation 2015. IAN Report 175, Band 1, Institut für Alpine Naturgefahren, Universität für Bodenkultur – Wien.

Immerzeel, W. W., Kraaijenbrink, P. D. A., Shea, J. M., Shrestha, A. B., Pellicciotti, F., Bierkens, M. F. P., & de Jong, S. M. (2014). High-resolution monitoring of himalayan glacier dynamics using unmanned aerial vehicles. *Remote Sensing of Environment, 150*, 93–103. https://doi.org/10.1016/j.rse.2014.04.025.

Jaboyedoff, M., Oppikofer, T., Abellan, A., Derron, M. H., Loye, A., Metzger, R., & Pedrazzini, A. (2012). Use of LIDAR in landslide investigations: A review. *Natural Hazards, 61*(1), 5–28. https://doi.org/10.1007/s11069-010-9634-2.

Lague, D., Brodu, N., & Leroux, J. (2013). Accurate 3D comparison of complex topography with terrestrial laser scanner: Application to the Rangitikei canyon (N-Z). *ISPRS Journal of Photogrammetry and Remote Sensing, 82*, 10–26. https://doi.org/10.1016/j.isprsjprs.2013.04.009.

Lindner, G., Schraml, K., Mansberger, R., & Hübl, J. (2016). UAV monitoring and documentation of a large landslide. *Appl Geomat, 8*(1), 1–11. https://doi.org/10.1007/s12518-015-0165-0.

Lucieer, A., de Jong, S. M., & Turner, D. (2014). Mapping landslide displacements using structure from motion (SfM) and image correlation of multi-temporal UAV photography. *Progress in Physical Geography, 38*(1), 97–116. https://doi.org/10.1177/0309133313515293.

Mateos, R. M., Azañón, J. M., Roldán, F. J., Notti, D., Pérez-Peña, V., Galve, J. P., Pérez-García, J. L., Colomo, C. M., Gómez-López, J. M., Montserrat, O., Devantèry, N., Lamas-Fernández, F., & Fernández-Chacón, F. (2017). The combined use of PSInSAR and UAV photogrammetry techniques for the analysis of the kinematics of a coastal landslide affecting an urban area (SE Spain). *Landslides, 14*(2), 743–754. https://doi.org/10.1007/s10346-016-0723-5.

Mazzanti, P. (2012). Remote monitoring of deformation. An overview of the seven methods described in previous GINs, Geotechnical News, December 2012, 24–29, ISSN: 0823-650X.

Mazzanti, P. Pezzetti, G. (2013). Traditional and innovative techniques for landslide monitoring: dissertation on design criteria. 19. Tagung für Ingenieurgeologie mit Forum für junge Ingenieurgeologen, pp. 191–197.

Nebiker, S., Annen, A., Scherrer, M., & Oesch, D. (2008). A light weight multispectral sensor for micro UAV—opportunities for very high resolution airborne remote sensing. *Proceeding of the The International Archives of the Photogrammetry, Remote Sensing and Spatial Information Sciences, XXXVII*(Part B1. Beijing), 1193–1199.

Niethammer, U., Rothmund, S., & Joswig, M. (2009). UAV-based remote sensing of the slow-moving landslide super-Sauze. In J.-P. Malet, A. Remaître, & T. Boogard (Eds.), *Proceedings of the International Conference on Landslide Processes: From geomorphologic mapping to dynamic modelling* (pp. 69–74). Strasbourg (2009: CERG Editions.

Peterman, V. (2015). Landslide activity monitoring with the help of unmanned aerial vehicle. The International Archives of the Photogrammetry, Remote Sensing and Spatial Information Sciences, Volume XL-1/W4, 2015 International Conference on Unmanned Aerial Vehicles in Geomatics, 30 Aug–02 Sep 2015, Toronto, Canada, pp. 215–218.

Peternal, T., Kumelj, S., Ostir, K., & Komac, M. (2017). Monitoring the Potoška planina landslide (NW Slovenia) using UAV photogrammetry and tachymetric measurements. *Landslides, 14*(1), 395–406. https://doi.org/10.1007/s10346-016-0759-6.

Savvaidis, P.D. (2003). Existing landslide monitoring systems and techniques. In Proceedings of the Conference from Stars to Earth and Culture, In honor of the memory of Professor Alexandros Tsioumis. Thessaloniki, Greece, pp. 242–258.

Scaioni, M. (2015). Modern Technologies for Landslide Monitoring and Prediction. *Springer Natural Hazards, 2015*, 249.

Schweigl, J. (2014). Hollenstein/Ybbs, Gst. Nr. 586, 663, 673. 659/1, 672/1 und 1263/5 (L6180) der KG Großhollenstein, Winkelmayer Karl u. Kordula, Fellner Dietmar, Katastrophenschaden, Erdrutsch und Mure, Wiederherstellung der Forststraße, Geologisches Gutachten (BD1-G-212/022–2014), Amt der Nieder- österreichischen Landesregierung, S. 3–4.

Shervais, K. (2015). Structure from Motion, Introductory Guide. Retrieved July 27, 2016, from https://www.unavco.org/education/resources/educational-resources/lesson/field-geodesy/module-materials/sfm-intro-guide.pdf.

Snavely, N., Seitz, S. M., & Szeliski, R. (2008). Modeling the world from internet photo collections. *International Journal of Computer Vision, 80*(12), 189–210. https://doi.org/10.1007/s11263-007-0107-3.

Stumpf, A. (2013). Landslide recognition and monitoring with remotely sensed data from passive optical sensors. PhD Thesis, University of Strasbourg.

Sugiura, R., Noguchi, N., & Ishii, K. (2007). Correction of low-altitude thermal images applied to estimating soil water status. *Biosystems Engineering, 96*(3), 301–313. https://doi.org/10.1016/j.biosystemseng.2006.11.006.

Tanteri, L., Rossi, G., Tofani, V., Vannocci, P., Moretti, S., Casagli, N. (2017). Multitemporal UAV survey for mass movement detection and monitoring. M. Mikoš et al. (eds.), Advancing culture of living with landslides. DOI https://doi.org/10.1007/978-3-319-53498-5_18.

Turner, D., Lucieer, A., & de Jong, S. M. (2015). Time series analysis of landslide dynamics using an unmanned aerial vehicle (UAV). *Remote Sensing, 7*(2), 1736–1757. https://doi.org/10.3390/rs70201736.

Ullman, S. (1979). The interpretation of structure from motion. Proc. R. Soc. London, Ser. *B, 203*(1153), 405–426. https://doi.org/10.1098/rspb.1979.0006.

Vrublová, D., Kapica, R., Jiránková, E., & Struś, A. (2015). Documentation of landslides and inaccessible parts of a mine

using an unmanned UAV system and methods of digital terrestrial photogrammetry. *GeoScience Engineering, 61*(3), 8–19.

Wallace, L., Lucieer, A., Watson, C., & Turner, D. (2012). Development of a UAV-LiDAR system with application to forest inventory. *Remote Sensing, 4*(12), 1519–1543. https://doi.org/10.3390/rs4061519.

Watts, A. C., Ambrosia, V. G., & Hinkley, E. A. (2012). Unmanned aircraft systems in remote sensing and scientific research: Classification and considerations of use. *Remote Sensing, 4*(12), 1671–1692. https://doi.org/10.3390/rs4061671.

Warrick, J. A., Ritchie, A. C., Adelman, G., Adelman, K., & Limber, P. W. (2017). New techniques to measure cliff change from historical oblique aerial photographs and structure-from-motion photogrammetry. *Journal of Coastal Research, 33*(1), 39–55.

Wieczorek, G. F., & Snyder, J. B. (2009). Monitoring slope movements. In R. Young & L. Norby (Eds.), *Geological monitoring: Boulder* (pp. 245–271). Geological Society of America: Colorado.

Xiang, H., & Tian, L. (2011). Development of a low-cost agricultural remote sensing system based on an autonomous unmanned aerial vehicle (UAV). *Biosystems Engineering, 108*(2), 174–190. https://doi.org/10.1016/j.biosystemseng.2010.11.010.

Zhou, G., Zang, D. (2007). Civil UAV system for earth observation. Proc. IGARSS, pp. 5319–5322.